Catena 197 (2021) 104951

Contents lists available at ScienceDirect

Catena

journal homepage: www.elsevier.com/locate/catena

Reconsidering the compound effect of geomorphology, vegetation, and climate change on paleopedogenesis in sensitive environments (Northern Apennines, Italy)

A. Masseroli[a,*], S. Villa[b], G.S. Mariani[c], I.M. Bollati[a], M. Pelfini[a], D. Sebag[d,e,f], E.P. Verrecchia[d], L. Trombino[a]

[a] Department of Earth Sciences "A. Desio", Università degli Studi di Milano, Milano, Italy
[b] Dipartimento di Scienze Agrarie e Ambientali – Produzione, Territorio, Agroenergia, (DiSAA), Università degli Studi di Milano, Milano, Italy
[c] Dipartimento di Scienze Chimiche e Geologiche, Università degli Studi di Cagliari, Cagliari, Italy
[d] Institute of Earth Surface Dynamics, Faculty of Geosciences and the Environment, Université de Lausanne, Switzerland
[e] Normandie University, UNIROUEN, UNICAEN, CNRS, M2C, 76000 Rouen, France
[f] IFP Energies Nouvelles (IFPEN), Direction Géosciences, Rueil-Malmaison, France

ARTICLE INFO

Keywords:
Complex paleosols
Paleosols sequences
Rock-Eval® pyrolysis
Soil micromorphology
Slope dynamic
Northern Apennines

ABSTRACT

Complex sequences of paleosols are often formed by the interaction between pedogenesis and geomorphological evolution. Their study, particularly in mountain areas, is useful to reconstruct past environmental conditions as well as climate shifts, and to gather information on the morphodynamical processes affecting the landscape through time.

Since the combined role that all different factors can play in the soil formation and evolution through time and space influences the formation and evolution of those complex paleosol sequences, a multidisciplinary study was conducted at the NW slope of Mt. Cusna (Northern Apennines, Italy). This work aims to reconstruct and to evaluate how the interactions between the geomorphological context, the Holocene climate variations, and the modification of the vegetation cover and composition influence the soil development of this area.

A combination of routine soil analyses (i.e., grain-size distributions, total organic carbon, total nitrogen, pH, and Fe/Al extractions), soil micromorphology and the Rock-Eval® pyrolysis allowed to characterize and to correlate the different soil units constituting a toposequence of six soil profiles.

The presence of different pedological units that can be correlated along the slope underlines the occurrence of separate events of pedogenesis, spatio-temporally linked to recognizable stability phases at slope scale. These phases of biostasy, characterized by vegetation cover and soil development, alternate to phases of rhexistasy, characterized mainly by slope instability (i.e., aggradation/degradation).

In detail, in the Mt. Cusna toposequence three different soil units, linked to three different stability phases, have been identified: the earliest stability phase, characterized by the presence of well-developed Luvisols, the subsequent stability phase typified by less expressed Luvisols, and the ongoing stability phase with Leptosols. This latter pedogenetic phase, in some cases, is superimposed to the previous one, so affecting the exhumed paleosols.

In this light, the Mt. Cusna toposequence characterization allowed to enlighten the complexity of soil polygenesis in higher detail than the previous studies, not only reconstructing the past environmental conditions but also inferring the succession of phases of slope stability and phases characterized by erosion and deposition processes.

1. Introduction

Soil evolution in active landscapes, such as mountain environments, is mainly influenced and controlled by topography (Zanini et al., 2015). Slope dynamics and instability influence soil formation, development, and preservation: conditions of slope instability can dramatically impact on soil formation and conservation in both short and long terms (Bollati et al., 2019; Coltorti et al., 2019). Areas characterized by steep

* Corresponding author at: Earth Science Department "A. Desio", Università degli Studi di Milano, Via Mangiagalli, 34, 20133 Milan, Italy.
E-mail address: anna.masseroli@unimi.it (A. Masseroli).

https://doi.org/10.1016/j.catena.2020.104951
Received 28 January 2020; Received in revised form 22 August 2020; Accepted 3 October 2020

slopes are affected by frequent and, often, rapid mass movements related to gravity and water-driven processes, which are able to substantially disrupt the relief and modify the old surfaces and dismantling previous soils and paleosols (Dewolf and Bourrié, 2008). Slope processes can vary in frequency and intensity under changing climate, environmental conditions and anthropogenic influence, resulting in a succession of rhexistasy and biostasy phases (Erhart, 1967). Consequently, pedogenesis can be variously impaired over time, whether interrupted, and soils can be buried by deposition phases, or get partially or completely eroded. Moreover, during the successive stability phases, soil formation processes can restart under new environmental conditions. In this light, the result of this tight interaction between pedogenesis and geomorphological evolution is the formation of complex sequences of paleosols, which formed in different morphoclimatic environments associated to distinct paleosurfaces (Fedoroff et al., 1990; Coltorti and Pieruccini, 2006; Vittori Antisari et al., 2016). Therefore, an exhaustive investigation of such sequences of paleosols is useful to reconstruct past environmental conditions as well as climate shifts, and to gather information on the morphodynamic processes affecting the landscape through time (Ruellan, 1971; Magliulo et al., 2006; Sheldon and Tabor, 2009). This proxy, evidence of environmental changes recorded in soils and paleosols, is often used as a paleoenvironmental tool in the mountain areas (Kaiser et al., 2007; D'Amico et al., 2016), and specifically in the Apennines (Giraudi, 2005; Coltorti and Pieruccini, 2006; Magliulo et al., 2006).

In the Northern Italian Apennines, the area of Mt. Cusna has been investigated with an array of studies based on various approaches in order to reconstruct its climate and environmental history through the Holocene. Multidisciplinary paleoenvironmental studies carried out at the treeline (Compostella et al., 2013, 2014) helped in characterizing the climate history of the soils in the area. In addition, geoarchaeological investigations of Mesolithic sites allowed the past environmental conditions of the area to be described using soil data, archaeological evidences, and palynological studies (Biagi et al., 1980; Cremaschi et al., 1984). Two geomorphological maps, within a time distance of 25 years (Panizza et al., 1982; Mariani et al., 2018), were made with the aim of reconstructing the geomorphological evolution of the area through the representation of landforms and paleosurfaces and their reciprocal distribution. However, in the Mt. Cusna area, no studies have been focused yet on the combined role that all different soil formation factors (Jenny, 1941) could have played in soil formation and evolution through time and space.

Therefore, this work aims at the characterization and the correlation of different soil units constituting a toposequence (Milne, 1936) of six soil profiles at the NW slope of Mt. Cusna, by means of a combination of routine soil analyses (i.e., grain-size distributions, total organic carbon, total nitrogen, pH, and Fe/Al extractions), soil micromorphology and a non-conventional approach to interpret soil organic matter dynamics: the Rock-Eval® pyrolysis. Moreover, we focused on the information recorded in soils to try to reconstruct and evaluate how the interactions between the geomorphological context, the Holocene climate variations, the vegetation change and human impact influence the formation and evolution of the studied complex paleosol sequences.

2. Materials and methods

2.1. Geological, geomorphological and soilscape settings of the study area

The study area is located on the NW slope of Mt. Cusna (2120 m a.s.l.; Fig. 1a), the second highest peak of the Northern Italian Apennines. Mt. Cusna is located in the territory of Febbio (Emilia Romagna region), inside the "*Parco Nazionale dell'Appennino Tosco-Emiliano*" (Tuscan-Emilian Apennine National Park).

The climate is sub-Mediterranean with abundant and well distributed precipitation (2000 mm/y), with a summer minimum (Compostella et al., 2014). Mean annual temperatures range from 8.8 °C (Ligonchio, 928 m a.s.l., 44°31′N-10°35′E) to 2.2 °C (Mt. Cimone, 2165 m a.s.l., 44°21′N-10°70′E; observation period for both stations 1961–1990). The study area, located between 1600 and 1700 m a.s.l., is slightly below the current treeline position (1750 m a.s.l., Compostella et al., 2013), and it is characterized by an open deciduous forest dominated by beech (*Fagus sylvatica*). Sparse shrubs and grassland species are also present, mainly *Vaccinium myrtillus*, *Juniperus nana*, *Thymus* sp, and *Laburnum alpinum*.

The bedrock consists mainly of turbiditic sandstones (locally marlstones) with intercalated sequences of claystones and siltstones (Panizza et al., 1982; Bortolotti, 1992). This area was diffusely subject to glacial and periglacial processes during the last glacial phases as testified by the presence of cirques and till deposits in the surroundings and by the general rounded and hilly aspect of the slopes (Losacco, 1949, 1982; Mariani et al., 2018). During the Holocene, the most widespread processes are due to gravity and water runoff (Panizza et al., 1982; Mariani et al., 2018). The Mt. Cusna area is affected by extremely active slope morphodynamics (Bertolini and Pellegrini, 2001) as demonstrated by the presence of rock and debris slides on the slopes of the main ridges, with varying dimensions and positions (Mariani et al., 2018). Moreover, the areas of Mt. Cusna, where slopes are more stable and flat, are covered by wider colluvium deposits (Mariani et al., 2018).

In the study area, processes related to surface running water play also an important role in shaping the landforms, in different ways, according to the substrate. Runoff and wash out phenomena have low intensity on sandstone outcroppings, due to their semipermeable property. On the contrary, where claystones and marlstones outcrop, water runoff often exposes surfaces due to their mostly impermeable property, and large washout areas are characterized by the presence of pseudo-gullies (Mariani et al., 2018).

Given the widespread presence of degradation processes that have deposited substantial amounts of reworked sedimentary material and have eroded surfaces, the soil landscape is directly affected by the morphological conditions and evolution of the area. Consequently, around the study area, Entisols are found on active morphologies and mainly on claystones, Inceptisols developed on more stable surfaces, mainly on sandstones, whereas Spodosols are located at higher altitudes (Panizza et al., 1982). A detailed pedological map of the area is missing, but the 1:250000 soil map of Italy (Carta Ecopedologica d'Italia 1:250000, Servizi WMS, Geoportale Nazionale, http://www.pcn.minambiente.it/mattm/servizio-wms/) emphasizes the presence of Regosols or Cambisols (IUSS Working Group WRB, 2015).

Moreover, in the Mt. Cusna area traces of older soil formation, in the form of relict or buried paleosols, are also found below colluvial deposits. In particular, the most important paleosols associated to the Mt. Cusna paleosurface are located on the northern slope of Mt. Cusna (Panizza et al., 1982). These paleosols have been described as Tapto-Luvisols (Compostella et al., 2014 according to Krasilnikov and Calderón, 2006): these are mature soils, mainly subject to clay illuviation and with well differentiated horizons.

The first traces of human settlements in the area belong to Mesolithic hunters, between the Early and the Mid-Holocene (Mt. Bagioletto site, 1.6 km N far from the summit of Mt. Cusna; Panizza et al., 1982). Sporadic occupation is recorded from the Late Holocene to the Roman Age (Biagi et al., 1980; Panizza et al., 1982; Cremaschi et al., 1984). Later on, historical sources show a progressive colonization of the higher northern Apennines since the Late Middle Ages (Mariani et al., 2019a), with communities surviving on livestock and forest exploitation. Agriculture played a minor role and was limited to small patches nearest to settled villages (Panizza et al., 1982). During the last few centuries, farming has been mostly relegated below 1000–1300 m a.s.l., while higher altitudes were used for extensive utilization of the forests for wood and charcoal production; pastures occupied the highest altitudes, up to the Mt. Cusna peak.

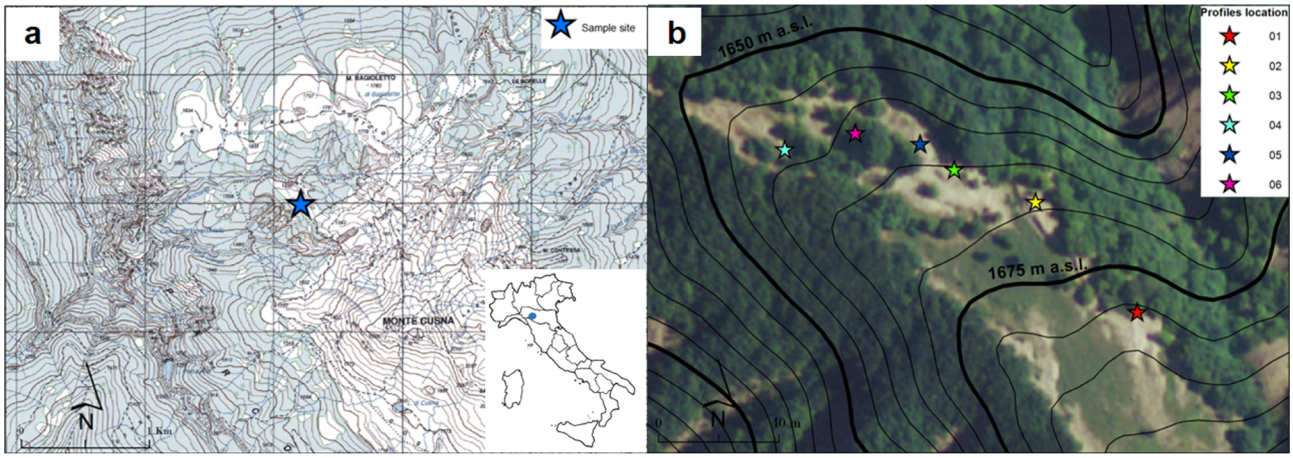

Fig. 1. a) Study area and location of the sample site at Mt. Cusna on altitude contour map. b) Locations of profiles on the orthophotograph (2006). The digital sources are courtesy made available by the Geoportale Nazionale (http://www.pcn.minambiente.it/GN/, WMS service).

2.2. Soil sampling

Six soil profiles were dug and described according to Jahn et al. (2006; Table 1) along an altitudinal transect on the NW slope of Mt. Cusna (Fig. 1b). Five soil profiles were chosen in an area as they were affected by running water erosion, whereas one soil profile (04) was excavated in a stable area with a forest plant cover. The locations of the five profiles were chosen on high topographic position, currently preserved from erosion processes. The coordinates of each profile were recorded using a GPS device. Between 0.5 and 2 kg of material were sampled from all identified soil horizons for laboratory analyses (Avery and Bascomb, 1982; Gales and Hoare, 1991; Cremaschi and Rodolfi, 1991). Seven undisturbed samples were collected using Kubiëna boxes (Kubiëna, 1953) from selected soil horizons to obtain thin sections for micromorphological investigations.

2.3. Soil analyses

Air-dried soil samples were treated by wet sieving in order to separate skeleton particles (> 2 mm) from the fine earth. The pH (in 1:2.5 soil: distilled water), total Organic Carbon (Org. C) content (Walkley and Black, 1934), and total nitrogen content (Kjeldahl, 1883) were measured for each soil sample. Particle size distributions were obtained on samples pretreated with H_2O_2 (130 volumes); sand fractions (from 2000 to 63 μm) were collected by sieving, while silt and clay particles (< 63 μm) were measured by aerometry with the Casagrande aerometer (Casagrande, 1934).

Different iron and aluminium forms were quantified (Ministero delle Risorse Agricole Alimentari e Forestali, 1994). Non-silicate forms ("free" iron, Fe_d and Al_d) were extracted with a bicarbonate-dithionite-citrate buffer, iron and aluminium in amorphous oxides and hydroxides ("active" forms, Fe_o and Al_o) were extracted with acid ammonium oxalate and, iron and aluminium bound to organic matter with covalent or partially polar bond (Fe_p and Al_p) were extracted in a solution of sodium pyrophosphate. For all forms, the amount of solubilized iron and aluminium in the supernatant was determined by means of a 4100 MP-AES (Agilent), after appropriate dilutions. Data with a %RSD (Relative Standard Deviation) of concentration > 3.5 and/or with a not detectable clear peak, were considered invalid (n.d. in Table 2), while the data close to the detection limit of the instrument were approximated to the minor concentration detectable (< n in Table 2).

In order to compare the results of iron and aluminium extractions to soil characteristics, both iron activity index (Fe_o/Fe_d) (Rhodes and Sutton, 1978) and illuviation (podzolization) index ($Al_o + ½Fe_o$) were calculated (IUSS Working Group WRB, 2015). Moreover, the amount of crystalline iron oxides (Fe_{cry}) was calculated as the difference between the dithionite- and the oxalate-extractable Fe ($Fe_{cry} = Fe_d\text{-}Fe_o$) (Bascomb, 1968; Pawluk 1972; Cremaschi and Rodolfi, 1991; Zanelli et al., 2007).

Organic Matter (OM) analysis was performed using a Rock-Eval® 6 pyrolyser (Vinci Technologies, France). About 60 mg of crushed material, previously sieved (< 2 mm), was analyzed for each horizon. Total Organic Carbon (TOC), Mineral Carbon (MINC), Hydrogen (HI) and Oxygen (OI) Indices were calculated by integrating the amounts of Hydrocarbon Compounds (HC), CO, and CO_2 produced during thermal cracking of OM and oxidative decomposition of carbonate, between defined temperature limits (Lafargue et al., 1998; Behar et al., 2001). The I-index and R-index were computed according to Sebag et al. (2016). By construction, the R-index relates to the most thermally resistant and refractory pools of organic matter, while the I-index is related to the ratio between thermally labile and thermally resistant pools (see details in Sebag et al., 2016). As they arise from a mathematical composition, these two indexes may be inversely correlated to each other when OM stabilization results from progressive decomposition of organic components according to their biogeochemical stability. Previous studies show that this property is verified with both indices highly correlated along a constant line ("humic trend") in composts and undisturbed soil profiles (Albrecht et al., 2015; Matteodo et al., 2018; Schomburg et al., 2018, 2019; Sebag et al., 2016). For comparison, we used the Matteodo's dataset composed of 46 soil profiles selected across various ecounits in Swiss Alps (Matteodo et al., 2018). The "humic trend" equations in the I-index/R-index plot was calculated starting from both Matteodo's dataset and study area datataset (colored dots in Fig. 3b).

Finally, as shown in previous studies (Malou et al. 2020; Thoumazeau et al., 2020), a Delta I-index can be calculated: it refers to the difference between the I-index value of each sample and the I-index value calculated with the "humic trend" equation (in bold in Fig. 3b), calculated starting from study area sample data, at the R-index value of each sample.

2.4. Micropedology

Uncovered soil thin sections were prepared from undisturbed samples through impregnation with polystyrene. Thin sections were then observed by means of a petrographic microscope (Leica Laborlux 18 POL), in parallel (PPL), cross-polarized (XPL), and oblique incident light (OIL), using different objectives (1.6×, 4×, 10× and 25×). Thin sections were described according to Stoops (2003). The interpretation of thin sections was performed according to Stoops et al. (2018).

Table 1
Site description of investigated soil profiles.

Profile	Elevation (m a.s.l.)	Slope gradient (°)	Slope exposure	Profile exposure	Parent Material	Geomor-phological context	Vegetation
01	1680	10	NE	SW	Colluvium deposits composed of claystones	Middle slope, flank of residual hills preserved from water runoff	Semi-deciduous shrub mainly composed of *Vaccinium myrtillus* and *Juniperus nana*. Sparse arboreal vegetation is characterized by *Fagus sylvatica* and rare *Laburnum alpinum*
02	1669	2	N-NW	SW	Colluvium deposits composed of claystones	Middle slope, flank of residual hills preserved from water runoff	Semi-deciduous shrub mainly composed of *Vaccinium myrtillus* and *Juniperus nana*. Rare *Fagus sylvatica*
03	1665	4	NW	N	Colluvium deposits composed of claystones	Middle slope, portion of residual hills preserved from water runoff	Semi-deciduous shrub mainly composed of *Vaccinium myrtillus* and *Juniperus nana*. Rare *Fagus sylvatica*
04	1659	11	NW	N-NE	Colluvium deposits composed of claystones	Middle slope	Deciduous woodland composed of *Fagus sylvatica* with *Vaccinium myrtillus* undergrowth
05	1663	10	NW	N-NE	Colluvium deposits composed of claystones	Middle slope	Semi-deciduous shrub mainly composed of *Vaccinium myrtillus*
06	1661	22	S-SE	SW	Colluvium deposits composed of claystones	Middle slope, portion of residual hills preserved from water runoff	Semi-deciduous shrub mainly composed of *Vaccinium myrtillus*

3. Results

3.1. Soil profiles description and analyses

All the soil profiles are located between 1600 and 1700 m a.s.l. (Fig. 1b); five soil profiles (01; 02; 03; 05; 06) are located in areas affected by running water erosion (Table 1). The vegetation cover is composed of semi-deciduous shrubs in all the area of soil profiles, except for profile 04 characterized by beech forest.

Total depths for all profiles range from around 50 to about 180 cm. The thickest profiles are characterized by the presence of two (01) or three (02, 06) distinct soil units, identifiable in the field by the presence of grain-size discontinuities or buried organic horizons, and/or a color change. Soil structure is moderately expressed by granular or subangular blocky aggregates. Sometimes, surface horizons (i.e., 05 A, 06 O and 06 OA) exhibit only a single-grained structural condition. On the contrary, well separated angular blocky peds can be found in buried horizons. Colors range between 10YR and 2.5Y in their hue, with a tendency for chroma to increase with depth inside each single soil unit (see Appendix A for detailed data). All the profiles are characterized by acidic conditions ranging from pH 4 to 5.6, usually increasing with depth, except for surface O horizons, which are often less acid than the underlying horizon (Fig. 2).

Particle size distributions of the investigated soil profiles display some common traits. Silt is always the predominant fraction, ranging from 44% to about 65%, with variable amounts of clay (from 21% to 52%). On the contrary, gravels never exceed 5%, while sands are only rarely > 20% (Fig. 2). Moreover, the grain size distributions allow the presence of different soil units to be confirmed. Indeed, the 01 and 06 soil profiles show an increase in clays at the top of the buried units (e.g., in profile 01: clay increases by 13.2% between horizons BC and 2AB1; in profile 06: clay increases by 13.7% between horizons OA and 2AB1); on the contrary, the 02 soil profile displays an increasing clay content by 2.6% between the horizons 2AB and 2Btg. 03 and 05 profiles are characterized by a clay increase in the B horizons (i.e., 03 OB, 05 ABt1 and ABt2), whereas an increase of coarse materials clearly appears in correspondence of the topographic surface (03 OA and 05 A) and the deepest (03 BC) horizons (see Appendix B for detailed data and Appendix C for cumulative particle size distribution curves). Lastly, the 04 soil profile, under a stable forested area, shows a constant increase of the coarse fractions (gravel and sand) with depth (Fig. 2).

The identified discontinuities are also marked by the results from chemical analyses. Indeed, a peak of total organic C content is found at the top horizon of each buried unit in correspondence of the above-mentioned discontinuities: 01 2AB1, 06 3AB, 02 2AB, and in the horizon 02 3AB, while in the horizon 06 2AB1 a total N peak is found (Fig. 2). Conversely, in profile 04, total organic C decreases from the surface horizon with depth, as expected in conventional soil profiles. The same trend can be observed in profiles 03 and 05, with the exception of the OB horizon of 03, which shows an increase in total organic C, and the A horizon of 05, which has a more marked decrease in total organic C than the deeper horizons (Fig. 2).

In the analyzed soil profiles, the total N content follows roughly the same trend as the total organic C (Fig. 2), but with significantly lower values. In surface horizons, total organic C ranges between 14.7 g/kg (02) and over 100 g/kg (04 and 05), while total N content never exceeds 7.0 g/kg. When focusing on superficial OM-rich horizons, the highest total N contents (about 7 g/kg) are found in 01, 04 and 06, while the lowest values belong to 02 (about 1.4 g/kg), following the same trends as total organic C.

The total content of free iron oxides (Fe_d) in four horizons (01 2AB2, 03 OB, 05 ABt2 and 06 2AB1) exceeds 30 g/kg but this parameter generally ranges between 10 and 20 g/kg (Table 2). The values of amorphous iron oxides (Fe_o) tend to be lower (< 0.90–15.73 g/kg), as well as iron bound with organic matter (Fe_p), which ranges between < 3.00 and 15.98 g/kg. Regarding the aluminium content, its

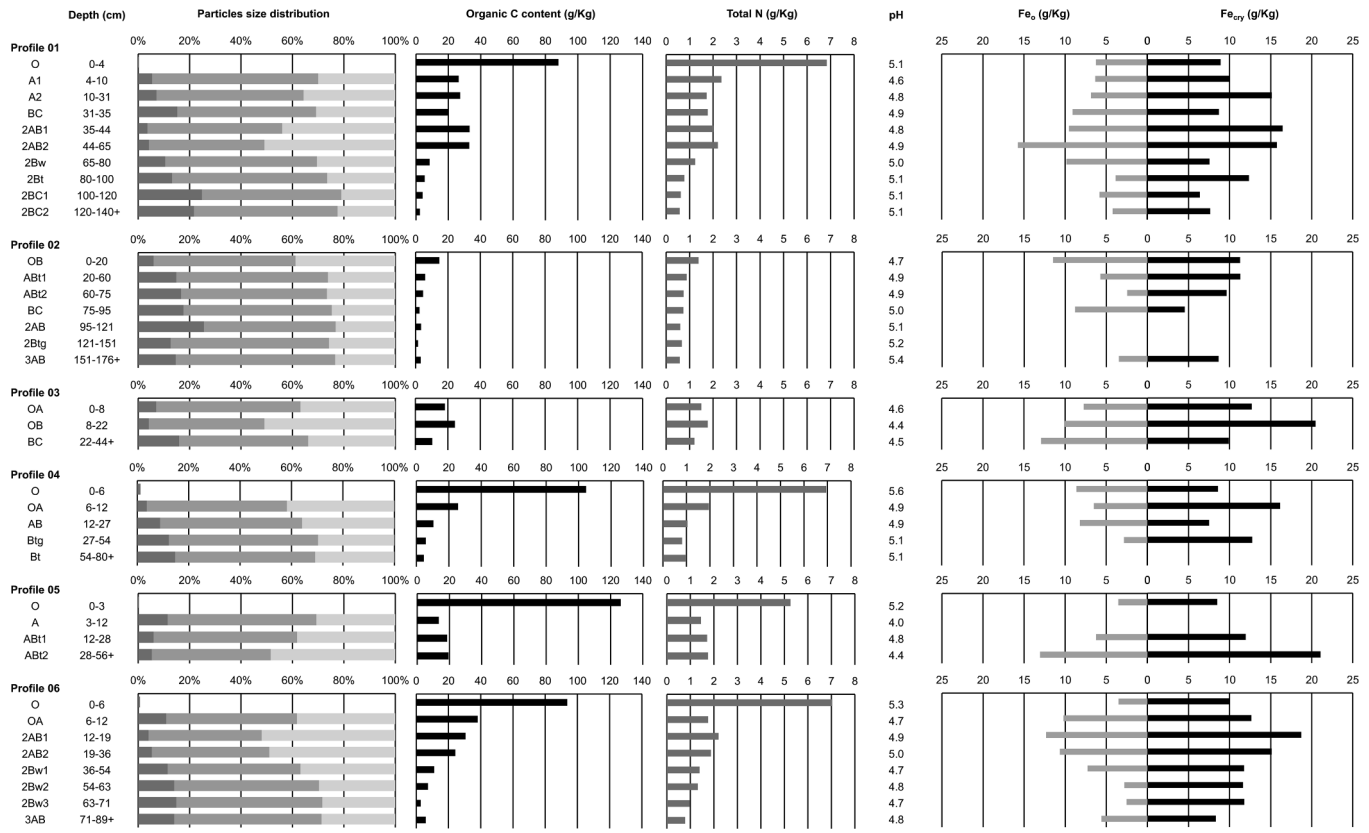

Fig. 2. Particle size distribution (dark grey: sand*; grey: silt; light grey: clay), organic C content, total N content, pH, contents in crystalline iron oxides (Fe_{cry}) and ammonium oxalate extractable Fe (Fe_o) in the studied profiles. The Fe_o is recognized as a measurement of the "activity" of iron oxides (Schwertmann, 1973). * Since the gravel content is very low, it has been added to the sand fraction.

values are lower and less variable than those of iron, with the exception of aluminium bound with the organic matter (Al_p) (Table 2). Free aluminium oxides (Al_d) reaches abundance from 2.64 to 5.83 g/kg, amorphous aluminium oxides (Al_o) from 0.85 to 5.59 g/kg, and the aluminium bound with the organic matter (Al_p) from 2.98 to 12.09 g/kg. The crystalline iron oxides (Fe_{cry}) are mainly concentrated in the B horizons (Fig. 2), and the highest value is found in the 05 ABt2 (21.08 g/kg). Along the profiles, the amorphous iron oxides (Fe_o) exhibit an opposite changing compared to crystalline iron oxides (Fig. 2), except for some superficial horizons (e.g., 06 OA) and in a few buried organic horizons (e.g., 01 2AB2). Indeed, in most of the profiles, the amorphous iron oxides show the lowest concentrations in Bt, Btg and partially in Bw horizons (Table 2; Fig. 2).

The iron activity index ranges from 0.18 to 0.66. In more detail, its lowest values are found in the Bt, Btg and Bw horizons (Table 2), in particular, in the B horizons of buried soils (e.g., 01 2Bt, 06 2Bw2 and 06 2Bw3). Instead, the BC horizons show the highest values of the iron activity index (e.g., 02 BC, 03 BC).

Finally, the results of the podzolization index ($Al_o + 1/2\ Fe_o$) partially meet the conditions for the presence of some podzolization processes only in the profile 02 (ABt2 and BC horizons; Table 2).

Rock-Eval® indices and parameters (Fig. 3; see Appendix B for detailed data) show that all the superficial organic horizons are plotted at the top left of the HI/OI diagram (Fig. 3a), whereas the buried soils are located at the bottom right of the diagram. Moreover, in the I/R diagram (Fig. 3b) the superficial organic horizons correspond to low R-index values and high I-index values and are located at the top left of the I/R diagram, whereas the organo-mineral and mineral horizons have a R-index values > 0.65 and are located in the right portion of the diagram. Taking into consideration the organo-mineral and mineral horizons in the I/R diagram, two different trends can be recognized. A first trend groups the horizons belonging to the superficial units of the soil profiles, which have I-index values varying between -0.3 and 0 (colored dots in Fig. 3b), whereas a second trend groups the horizons belonging to the buried units, which have higher I-index values, ranging from -0.2 to 0.5 (colored diamonds in Fig. 3b), except for horizons 01 2AB1, 2AB2 and 06 2AB1, 2AB2. On the other hand, some horizons from the superficial units are characterized by high I-index values (02 BC, ABt1 and ABt2; 04 Bt, Btg, AB; 03 BC). Moreover, when comparing R-index with depth, buried soils evidence a different trend; indeed, the 01 buried soil display R index values higher than the 02 buried soil, at the same depth and with similar TOC contents (Fig. 4a, b). The presence of two different trends can also be observed when taking into consideration the I-index/TOC diagram: the horizons belonging to the first trend show an expected increase of the I-index with TOC and a decrease with depth, whereas the horizons belonging to the second trend have (i) high I-index values even with low TOC and (ii) I-index values which are not decreasing with depth (Fig. 4c, d). Finally, horizons belonging to the second trend have high delta-I values (Fig. 4e), which means that the I-index values are high compared to those expected for the corresponding R-index values, when referring to the humic trend.

3.2. Soil thin sections micromorphology

The micromorphological observations were carried out on four out of the six examined profiles: 01, 02, 04 and 05 (see Appendix D for detailed thin sections descriptions). Horizons 02 ABt1, 01 2Bt and 04 Bt show some similar features: they all are characterized by granular aggregates of fine material and angular-subangular blocky aggregates, together with Fe-Mn nodules and well-developed clay coatings. Moreover, in the 02 ABt1, reworked soil fragments of subangular aggregates of fine material (i.e., pedorelicts *sensu* Brewer, 1976) with a high degree clay illuviation, and few allochthonous weathered rock

Table 2
Ammonium oxalate (Fe_o, Al_o), dithionite-citrate-bicarbonate (Fe_d, Al_d) and sodium pyrophosphate (Fe_p, Al_p) extractable Fe and Al in the studied profiles and derivate indices of crystalline iron oxides (Fe_{cry}), activity iron index (Fe_o/Fe_d) and podzolization index ($Al_o + 1/2Fe_o$). < : low values approximate to the minor concentration detectable; n.d.: no data.

Profile	Horizon	Depth (cm)	Fe_o (g/Kg)	Al_o (g/kg)	Fe_d (g/kg)	Al_d (g/kg)	Fe_p (g/kg)	Al_p (g/kg)	Fe_{cry} (Fe_d-Fe_o) g/kg	Feo/Fed	$Al_o + 1/2Fe_o$ %
01	O	0–4	6.24	2.87	15.16	3.65	4.70	11.41	8.91	0.41	0.60
	A1	4–10	6.33	3.46	16.39	4.09	5.81	8.67	10.06	0.39	0.66
	A2	10–31	6.84	3.29	21.99	4.88	6.24	10.90	15.15	0.31	0.67
	BC	31–35	9.08	4.40	17.78	4.13	5.54	6.62	8.70	0.51	0.89
	2AB1	35–44	9.52	2.74	25.98	4.37	9.70	8.50	16.46	0.37	0.75
	2AB2	44–65	15.73	4.44	31.47	5.71	15.98	10.37	15.74	0.50	1.23
	2Bw	65–80	9.84	5.06	17.39	5.05	7.44	7.46	7.55	0.57	1.00
	2Bt	80–100	3.85	2.88	16.20	4.97	4.10	6.09	12.35	0.24	0.48
	2BC1	100–120	5.80	4.30	12.17	4.17	< 3.00	4.86	6.37	0.48	0.72
	2BC2	120–140 +	4.19	3.45	11.82	4.00	n.d.	3.99	7.63	0.35	0.55
02	OB	0–20	11.49	4.02	22.76	4.44	8.68	7.46	11.27	0.50	0.98
	ABt1	20–60	5.73	3.45	17.01	5.16	n.d.	6.92	11.29	0.34	0.63
	ABt2	60–75	2.48	3.16	12.12	3.17	n.d.	3.84	9.64	0.20	0.44
	BC	75–95	8.82	5.40	13.37	3.62	n.d.	4.57	4.55	0.66	0.98
	2AB	95–121	< 0.90	1.69	12.70	3.07	n.d.	3.32	n.d.	n.d.	n.d.
	2Btg	121–151	n.d.	0.85	14.35	3.27	n.d.	3.64	n.d.	n.d.	n.d.
	3AB	151–176 +	3.48	2.40	12.14	2.84	n.d.	2.98	8.66	0.29	0.41
03	OA	0–8	7.73	3.39	20.43	4.10	6.21	7.08	12.70	0.38	0.73
	OB	8–22	10.11	2.74	30.57	4.25	12.26	9.42	20.47	0.33	0.78
	BC	22–44 +	12.92	5.59	22.82	5.53	8.53	6.30	9.89	0.57	1.21
04	O	0–6	8.61	3.13	17.21	3.38	4.58	4.34	8.60	0.50	0.74
	OA	6–12	6.48	3.17	22.61	4.85	8.23	8.52	16.14	0.29	0.64
	AB	12–27	8.19	4.93	15.70	4.62	5.17	7.58	7.51	0.52	0.90
	Btg	27–54	2.82	2.64	15.57	4.53	< 3.00	6.13	12.75	0.18	0.40
	Bt	54–80 +	n.d.	n.d.	14.37	3.68	< 3.00	4.52	n.d.	n.d.	n.d.
05	O	0–3	3.52	2.14	12.02	2.64	n.d.	3.42	8.49	0.29	0.39
	A	3–12	n.d.	n.d.	17.52	4.85	< 3.00	6.53	n.d.	n.d.	n.d.
	ABt1	12–28	6.24	2.71	18.21	3.45	5.63	6.38	11.97	0.34	0.58
	ABt2	28–56 +	13.06	3.78	34.13	5.83	13.27	12.09	21.08	0.38	1.03
06	O	0–6	3.52	2.12	13.44	4.02	< 3.00	4.58	9.92	0.26	0.39
	OA	6–12	10.21	4.53	22.84	4.53	7.15	7.69	12.64	0.45	0.96
	2AB1	12–19	12.34	3.28	31.07	5.60	12.72	9.31	18.73	0.40	0.94
	2AB2	19–36	10.66	3.73	25.79	5.49	12.63	7.95	15.13	0.41	0.91
	2Bw1	36–54	7.28	4.39	19.03	5.72	7.54	9.21	11.76	0.38	0.80
	2Bw2	54–63	2.82	2.29	14.45	4.43	< 3.00	7.30	11.63	0.20	0.37
	2Bw3	63–71	2.55	2.75	14.35	4.25	n.d.	3.92	11.80	0.18	0.40
	3AB	71–89 +	5.60	3.77	13.94	3.66	n.d.	4.52	8.33	0.40	0.66

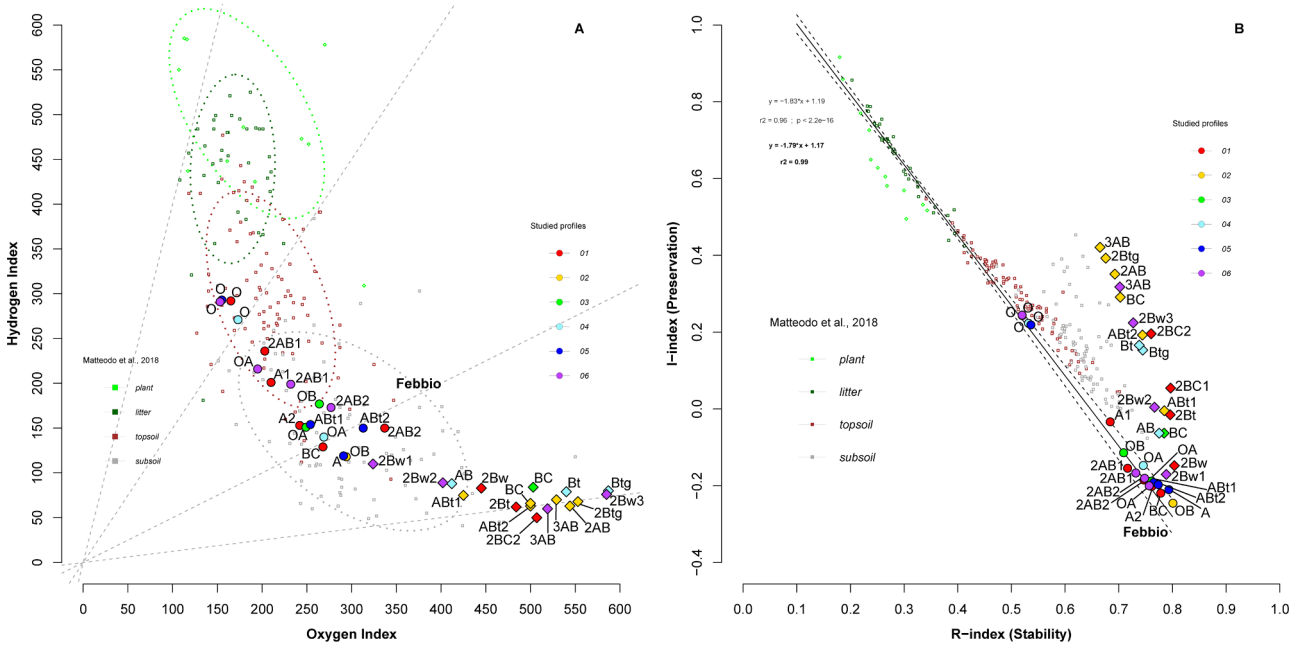

Fig. 3. a) HI (mg HC/g TOC)/OI (mg CO_2/g TOC) diagram; the horizon 01 2BC1 is not plotted due to its out of range value, b) I-index/R-index diagram of the studied horizons. Colored dots are used to calculate the "humic trend" equation written in bold. In background, the Matteodo's dataset, composed of 46 soil profiles selected across various ecounits in Swiss Alps (Matteodo et al., 2018) and the relating "humic trend" equation is depicted, as comparison.

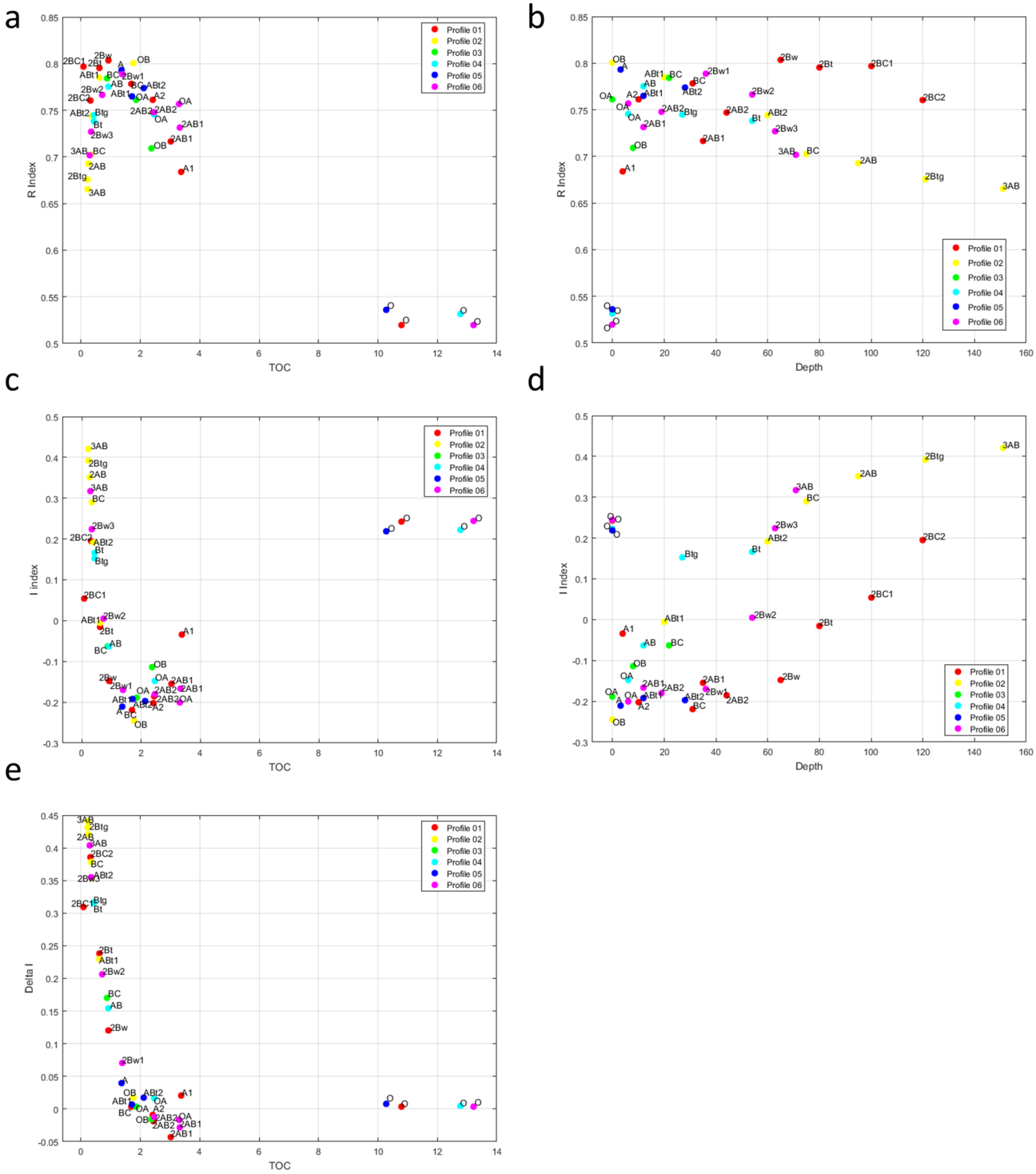

Fig. 4. a) R-Index/TOC (%) diagram; b) R-index/depth (cm) diagram; c) I-Index/TOC (%) diagram; d) I-index/depth (cm) diagram; e) Delta I/TOC (%) diagram of the studied horizons.

fragments are present (i.e., lithorelicts *sensu* Brewer, 1976). Furthermore, regarding the coarse mineral fraction, there are similar proportions of sandstone and claystone fragments in 02 ABt1 and 04 Bt, while in the 01 2Bt sandstone constitutes the prevalent lithology of fragments.

Similarly, 01 2AB1 and 2AB2, 05 ABt1 and ABt2 and 04 Btg horizons show analogous characteristics, such as their complex microstructure including granules and reddish clayey subangular aggregates, which contain a high proportion of Fe-Mn nodules (Fig. 5a, b). Moreover, the 01 2AB1 horizon differs from the 2AB2 horizon by the predominant sub-angular aggregates in the latter. Finally, in the 05 ABt1 and ABt2 and 04 Btg horizons show the presence of clay illuviation features (coatings); in the latter horizon, hydromorphic features in the form of depletion pedofeatures and intercalations are also found.

The micromorphological approach further underlines the presence of peculiar characteristics in 01 A2, BC and 2AB1 and 02 2Btg horizons. For example, the 02 2Btg horizon exhibits a compact, vughy

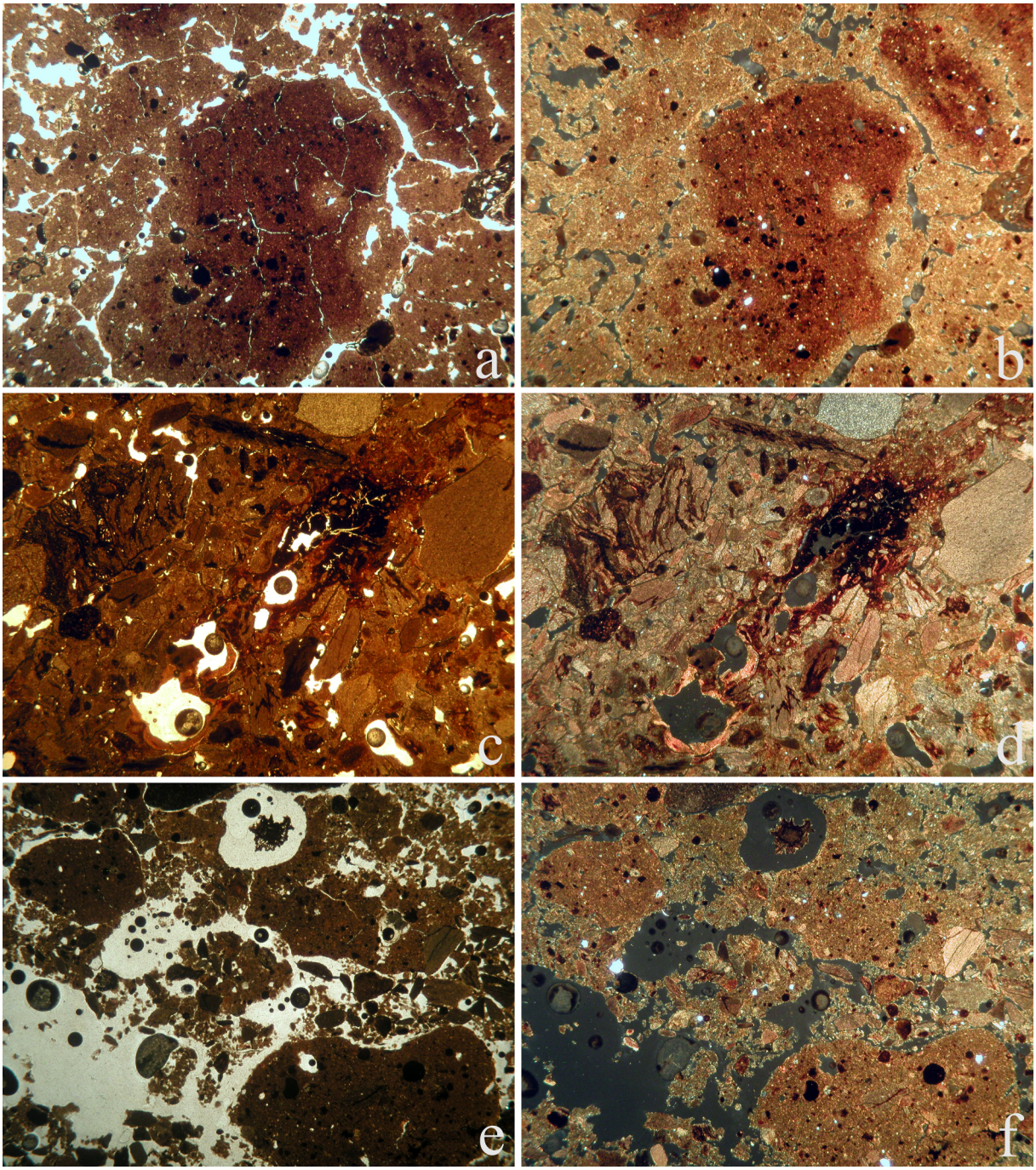

Fig. 5. Photomicrographs of some micromorphological features observed in soils and palaeosols. a,b) altered, reddish fine-material forming subangular aggregates, with Fe/Mn nodule concentrations in 05 ABt1 and ABt2 horizons (1.6×, PPL e XPL; field length: 8 mm); c, d) vughy structure with clay illuviation and redoximorphic features in a 02 2Btg thin section (1.6×, PPL and XPL; field length: 8 mm); e, f) crumb aggregates and reddish, subangular pedorelicts in the horizon BC of the 01 profile (1.6×, PPL e XPL; field length: 8 mm).

microstructure, and, well-developed diversified pedofeatures, such as dense digitate Fe-Mn nodules, typic clay coatings, typic clay infillings, and Fe-Mn hypocoatings (Fig. 5c, d).

Otherwise, the 01 A2, BC and 2AB1 horizons show a twofold distribution of crumbs and reworked subangular aggregates reddish in color, weakly striated and characterized by a high degree of pedogenesis (i.e., pedorelicts *sensu* Brewer, 1976). These pedofeatures are more common in the BC horizon (Fig. 5e, f). Finally, 01 2AB1 and 2AB2 contain identifiable pedofeatures only as Fe-Mn nodules, which are more concentrated inside the subangular reworked soil fragments.

4. Discussion

4.1. Complex paleosol sequences and the characterization of buried units

Sedimentological and chemical data help in identifying the presence and defining the boundaries of the soil units recognized in the field. Trend anomalies detected in analytical values are found in profiles 01 (between horizons BC-2AB1), 02 (between horizons BC-2AB and 2Btg-3AB), and 06 (between horizons OA-2AB1 and 2Bw3-3AB; Fig. 2). In horizons 2AB1 of 01, 2AB1 and 3AB of 06, high values of total organic C or total N contents as well as of fine material, underline the presence of

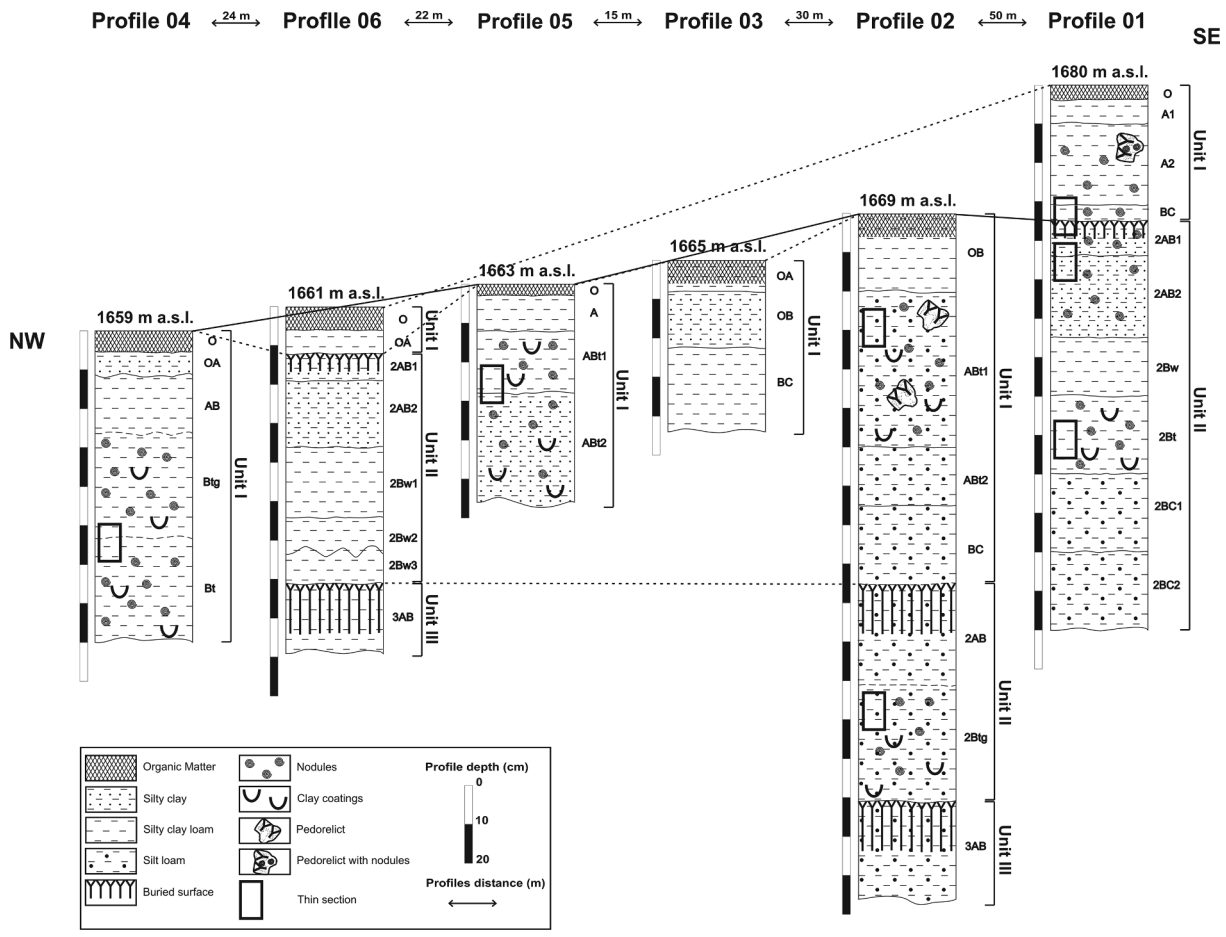

Fig. 6. Correlation scheme between the investigated soil profiles. The lines show the correlation among the different pedological units (black lines for the correlations found observing soil thin sections; dotted lines for the correlations supposed based on soil physical and chemical properties).

paleosurfaces, subsequently buried by coarse colluvial deposits, which disconnected the soils from surface pedogenetic processes (see below for micromorphological evidence). On the contrary, it is not possible to identify precisely in profile 02 the paleosurface location at the top of the 2AB horizon from the colluvial material above it. Even if the organic matter content peaks in 2AB horizon, both 2AB and BC horizons possess a high percentage of sand and gravel (Fig. 2). Moreover, both horizons in the field have a homogeneous aspect: it is possible that the distinction between these two units may be difficult to identify because of a higher energy of deposition of the colluvium, which mixed part of the materials during the process. In the same profile, the total organic C content allows a discontinuity at the top of the 3AB horizon to be identified (Fig. 2). The variations in particle size distributions within profiles 03, 04 and 05 are not attributed to the presence of paleosurfaces.

Micromorphological observations of thin sections from 01 and 02 profiles provide further information confirming the presence of different soil units and their respective characteristics. In 01, the presence of two distinct units is highlighted by the nature of the coarse material: in the surface unit (unit I) fragments of claystones are more abundant while in the deeper one (unit II), fragments of sandstones are more common. This difference in the coarse fraction lithology likely indicates the occurrence of two different parent materials, separating clearly two soil units. In unit II, weathering processes occurred in oxidative conditions with water infiltration, emphasized by the yellowish color of the groundmass indicating the presence of iron hydroxides (Sauro et al., 2009; Stoops et al., 2010, 2018; Compostella et al., 2014). The presence of clay illuviation features, indicated by clay coatings found in the 2Bt horizon, requires alternating phases of water infiltration into the soil, together with conditions of strong vegetative protection of the soil surface, in order to permit clay translocation into the deep horizons (McCarthy et al., 1998; Stoops et al., 2010, 2018). Moreover, the presence of Fe-Mn nodules indicates temporary waterlogging conditions inside the soil (McCarthy et al., 1998; Stoops et al., 2010, 2018), probably amplified by the presence of the underlying 2Bt horizon. The diffuse and irregular boundary of the nodules witnesses their *in situ* formation, without evidence of transport from other locations (Fedoroff and Goldberg, 1982). In unit I, frequent blocky peds show a generally reddish micromass color associated to Fe-Mn nodules, which indicate a degree of weathering greater than in the surrounding soil groundmass (e.g., reddish micromass, typic nodules of Fe-Mn and moderately weathered mineral fragments): therefore, these blocky peds can be regarded as pedorelicts (*sensu* Brewer, 1976), i.e., reworked fragments of an older soil (Fig. 5e, f) redeposited within more recent horizons (Kemp, 1998; Nicosia, 2006; Rellini et al., 2007; Sauro et al., 2009; Cremaschi et al., 2018). Moreover, these reworked fragments of paleosol are similar, in terms of fabric, to the 2AB2 horizon; thus, it is reasonable to state that they were eroded from higher portions of the slope and deposited within the presently BC horizon, which implies a highly erosive phase.

Regarding 02 profile, the micromorphological analysis indicates that the unit II (e.g., 2Btg horizon) is characterized by a stronger degree of pedogenesis than the unit I (e.g., ABt1 horizon). This is probably due to a greater intensity and/or duration of a pedogenetic phase. In unit II, clay coatings are clearly visible (Fig. 5c, d) and it is often possible to identify an orientation in the deposition of fine material due to the development of crescent internal fabric. This corroborates the hypothesis of transport of clay materials from upper horizons (McCarthy et al.,

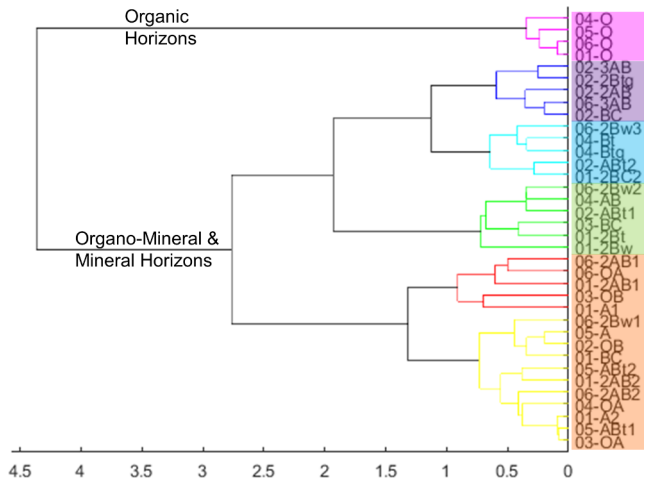

Fig. 7. Dendrogram output for clustering of studied horizons, using Rock-Eval indices (HI, OI, I-Index and R-Index). The horizon 01 2BC1 is not plotted due to its out of range values.

1998). Moreover, the 2Btg horizon is the only one showing the development of Fe-Mn hypocoatings, due to longer periods of waterlogging (McCarthy et al., 1998; Stoops et al., 2010). Finally, only rare reworked paleosol fragments (pedorelicts *sensu* Brewer, 1976), composed of clayey blocky peds, are found in the ABt1 horizon.

4.2. Correlation of soil units

As already described in Section 4.1 of the Discussion, the studied toposequence is constituted by six soil profiles located at different altitudes along the NW slope of Mt. Cusna, chosen according to their topographic position. Among the analyzed soil profiles, three are composed of different units, whereas only one soil unit is present in the other three profiles (03; 04 and 05).

In the following section, the most widespread unit set (i.e., unit II of 01; unit I of 02; 03; 04; 05; unit II of 06) is first characterized in order to better correlate the various soil profiles (Fig. 6). Indeed, the unit II of 01 (e.g., 2Bt) and the unit I of 02 (e.g., ABt1), although characterized by a different mineral component, are associated with the presence of clay illuviation and a very similar microstructure, together with the presence of moderately impregnated amorphous nodules. Therefore, these units could be formed by the same pedogenetic event on different parent materials, the latter deposited by distinct colluvial events.

Unit II of 01 can also be correlated with 05 profile (e.g., ABt1 and ABt2), which shows similar aggregates (both subangular blocky and granular) and microstructure with regard to the horizons 2AB1 and 2AB2 (01 profile), as well as clay illuviation features in the horizon 2Bt (01 profile). Moreover, moderate impregnative amorphous nodules of Fe-Mn are present through the referred horizons. The same consideration regarding microstructure, clay illuviation features, and amorphous nodules can be extended to the 04 profile, even if, in the horizon 04 Btg, the presence of hydromorphic features (i.e., depletion pedofeatures and intercalation, *sensu* Fedoroff and Courty, 2012) underlines a further pedogenetic phase induced by water logging, probably due to the topographic position.

The sedimentological and chemical data allow the above described correlation based on micromorphological features to be extended (Fig. 6): the unit II of the 01 (e.g., 2AB1 and 2AB2) and 06 (e.g., 2AB1 and 2AB2) profiles show the same clay high and sand low contents, and similar values of total organic C and total N contents. On the other hand, 03 profile can be correlated to the unit I of 02, not only because both units are characterized by a very low total organic C and total N contents, but also for their relative position along the slope.

In two profiles, 01 and 06, the above correlated unit is overlain by soil horizons, pointing to another soil unit (Fig. 6). This surficial unit, even if it is thin, shows uniform soil characteristics (particle size distributions, total organic C and total N contents), and could therefore be related to the same pedogenetic phase.

Focusing on soil horizons underlying the above correlated unit, the micromorphological observations highlight a general greater weathering impact. The 02 2Btg horizon (unit II) has very few analogies with the horizons observed in other profiles: the presence of well-developed pedofeatures (i.e., dense digitate nodules of Fe-Mn, typic clay coatings, typic clay infillings; and Fe-Mn hypocoatings) testifies a more intense pedogenetic phase, followed by a secondary hydromorphic phase induced by waterlogging. Moreover, the peculiarity of this unit II is also underlined by the organic matter thermal signature: in the R-index/depth plot, horizons of unit II from 02 have a lower R-index compared with the horizons belonging to unit II from 01, which are located at the same depth (Fig. 4b), due to a presence of different proportion of the most refractory organic pool (related to pedogenetic and inherited contributions) in the two units. A similar trend, though not so marked, is also visible in the R-index/TOC plot (Fig. 4a), where the horizons belonging to unit II of 02 are separated from the others. Furthermore, unit II of 02 may be correlated to unit III of 06 (Fig. 6). This deepest unit of 06 is only represented by a single horizon (3AB), but its stratigraphic continuity, in addition to Rock-Eval® parameters, suggest a possible correspondence between this unit and unit II of 02. Horizon 06 3AB is always located close to the horizons belonging to unit II of 02 in both R-index/TOC (Fig. 4a) and R-index/depth plots (Fig. 4b), underlining similar organic matter dynamics.

Regarding Rock-Eval® parameters, as discussed above, the HI/OI diagram emphasizes the way horizons belonging to unit II of 01 (red dots, 2AB1, 2AB2 in Fig. 3a) and unit II of 06 (violet dots, 2AB1, 2AB2 in Fig. 3a) group in the same set as the present-day surface horizons of all the profiles, while units II of 02 and III of 06 are located at the bottom right of the plot, probably due to the presence of an OM refractory pool. These horizon groupings are clearly distinguishable observing the results of cluster analysis (Fig. 7) carried out on the Rock-Eval® indices take into consideration (HI, OI, R-Index, I-Index): in the dendrogram it is possible to observe how the organic O horizons clearly differ from the organo-mineral and mineral horizons. Among the organo-mineral and mineral horizons, the horizons belonging to unit II of 01 and unit II of 06 group are grouped in the same set as the present-day surface horizons of all the other profiles (02, 03, 04 and 05), while units II of 02 and III of 06 are all grouped together, close to the deepest horizons of the other units (01 2BC2; 02 BC, ABt2; 04 Bt, Btg; 06 2Bw3) (Fig. 7). Moreover, the cluster analysis grouped the organo-mineral and mineral horizons in two different great groups, which can be attributable to a different evolution trend of organic matter. Indeed, in the I/R diagram (Fig. 3b), the #*B* horizons belong to the first set (i.e., 01 2Bw, 2Bt, 2BC1, 2BC2; 02 BC, 2AB, 2Btg, 3AB; 03 BC; 04 AB, Bt, Btg; 06 2Bw1, 2Bw2, 2Bw3, 3AB; colored diamonds in Fig. 3b; these horizons are not belonging solely to buried units) show a new trend, parallel to the "*Inherited Organic Matter Trend*" proposed by Sebag et al. (2016). On the other hand, horizons richer in organic matter (i.e., 01 A1, A2, BC, 2AB1, 2AB2; 02 OB; 03 OA, OB; 04 OA; 05 A, ABt1, ABt2; 06 OA, 2AB1, 2AB2; colored dots in Fig. 3b; these horizons belong to surface or buried units) fit the "*Humic Trend*" (Sebag et al., 2016; Matteodo et al., 2018).

This new identified trend, grouping #*B* horizons with a high degree of weathering observed in both surface and buried units, suggests the presence of a relationship between these different soil horizons. In these horizons, as already specified, the presence of features related to pedogenetic processes not in equilibrium with the present-day environmental conditions, clearly defines these soil horizons as parts of paleosols (i.e., relict soils *sensu* Ruellan, 1971). Moreover, this new trend clearly differs from the "*Humic trend*" (Sebag et al., 2016; Matteodo et al., 2018), mainly for what concerns the I-index values (Fig. 4c, e). Indeed, the horizons belonging to this trend show high I-index values (even if the TOC content is low; Fig. 4c, e), emphasizing

the relatively low contribution of resistant pool compared to the most labile pools. Similar results have been obtained when advanced decomposition of OM affects both thermally labile and resistant pools, as in Arenosols for example (Malou et al. 2020; Romanens et al., 2019). In the context of the present study, the decomposition of thermally resistant pools can be explained by an earlier phase of pedogenesis and this peculiarity of the trend supports the hypothesis that these soils located along the trend are paleosols. The presence in most of these horizons of high I-index values allows these horizons to be identified as former superficial ones, probably influenced in the past by the pedological surface processes involving organic matter. Moreover, their present day low TOC contents is explained when considering the geomorphological context of the area. In addition to advanced decomposition of OM, the contribution of mineral material, especially in these horizons, is due to colluvium deposition episodes affecting the slope. The presence of these truncated and buried units can be attributed to the interaction of erosive and depositional processes happening at different times and ultimately led by colluvial dynamics. The remix and redeposition of this loose material contributed to organic matter dilution, and, at the same time, buried soil units, isolating the soil by preventing the modification and external contributions to the buried organic matter.

Two type of paleosols can be observed: (i) buried soils (i.e., 01 2Bw, 2Bt, 2BC1, 2BC2; 02 2AB, 2Btg, 3AB; 06 2Bw1, 2Bw2, 2Bw3, 3AB), as considered soil units are buried, and (ii) exhumed paleosols (i.e., buried soils that have been brought to surface by erosion, *sensu* Cremaschi et al., 2018) (i.e., 02 ABt1, ABt2, BC; 03 BC; 04 AB, Bt, Btg), when considered soil units outcrop at the surface. Therefore, the new observed trend in the I/R diagram identifies some horizons of maximum weathering in the paleosols, regardless their morphological position, within the given limits of the study area. This specific paleosols trend in the I/R diagram represents a potential approach for further investigations regarding new criteria for paleosols identification.

Finally, regarding the iron and aluminium content, all analyzed Bt, Btg and Bw horizons show an increase in crystalline iron oxides (Fe_{cry}), underlining the expression of some pedogenesis at work (Table 2; Fig. 2). Furthermore, the iron activity index (Fe_o/Fe_d) shows a decrement within the most mature Bt, Btg and Bw horizons, likely emphasizing a stronger weathering (Table 2). Unfortunately, this ratio does not change significantly when comparing recent soils and paleosols; consequently, it is not wise to use it as a proxy for soil age (Arduino et al., 1986).

4.3. The role of geomorphological processes in the development of complex pedosequences

The presence of different pedological units, and their correlation along the slope, underlines the occurrence of separate events of pedogenesis, spatio-temporally related to recognizable stability phases at the slope scale. These phases of biostasy (Erhart, 1967) are characterized by the absence of erosion and/or deposition on the slope, a vegetation cover, and a soil development. They alternated with phases of rhexistasy (Erhart, 1967), characterized by slope instability. The study area has been affected by various colluvial events, as testified by trends in coarse materials content and the presence of pedorelicts and lithorelicts (*sensu* Brewer, 1976) in the surface units.

Moreover, the phases of rhexistasy strongly control the conditional conservation of soils along the slopes: higher energy conditions would produce excessive disruption along the slopes in form of increased colluvial and mass wasting events. These events would destroy the soil cover and cause the disappearance of evidences of previous pedogenetic phases in the area and at the same time inhibit the formation of new soils. However, even if these multiple phases of slope activity may have locally eroded part of the pre-existing soil cover (e.g., unit I of 02), at the same time, they locally buried parts of it, preserving some paleosols over time (e.g., unit II of 01). In addition, the geomorphological evolution of the slope through time may also brought previously buried paleosols to the surface again as a consequence of erosion, superimposing later a new pedogenetic phase on pre-altered materials, as attested by unit I of 02 and probably 03 and 05. In this sense, slope morphodynamics do not seem to influence directly the intensity of *soil formation processes*, but they act as a key factor controlling the distribution and occurrence of soil units and paleosols. Therefore, the development of the studied complex pedosequences is not the exclusive result of vertical top-down processes but of a number of complex processes including near-surface processes such as material sedimentation and erosion.

On account of this, in the study area the evidence of different colluvial deposits in these pedosequences shares similarities with coverbeds successions (Kleber and Terhorst, 2013), thought at a much smaller scale and magnitude.

4.4. Reconstruction of the environmental changes during the Holocene along the Mt. Cusna NW slope

From the pure pedogenetic point of view, three separate phases have been recorded inside the soil units all along the slope (Fig. 6). These three pedogenetic phases are preceded by another pedogenetic phase, which will not be discussed because, since it is represented by an only one horizon (02 3AB) and it is the first time that it is found, there is not enough information to carry out a detailed reconstruction of the pedogenetic processes that have affected it. From the oldest to the most recent, these three separate phases are identified as:

- *α pedogenesis*: it is observed exclusively in unit II of 02 (and partially in unit III of 06), and displays the characteristics of a well-developed brunification with clay illuviation (Duchaufour, 1983), high Fe_d content and clay increase in Btg horizon. This strongly expressed pedogenetic phase led to the formation of a Luvisol (IUSS Working Group WRB, 2015), developed under a forest vegetation cover, as evidenced by the yellowish brown matrix with speckled striated b-fabric (Douglas and Thompson, 1985) and by the pedofeatures (i.e., frequent typic clay coatings; rare crescent typic clay coatings; very few typic clay infillings) observed in thin sections. This phase was interrupted by a sudden deposition of colluvial material, mobilized upslope by water runoff. During this phase, the soil surface of the evolving soil was buried, interrupting its pedogenesis. During this runoff period, the slope was not likely covered by forests, as they would have effectively prevented such mass movements. Consequently, this colluvial event provided a new parent material for further soil development during the following phase;

- *β pedogenesis*: it is characterized by a moderately developed brunification with some clay illuviation (i.e., unit I of 02, unit II of 01, 05, and probably 03 and unit II of 06) in different parent materials. The presence of different parent materials is probably the results not only of various colluvial events, but also of a differentiated material deposition, both in quantity and composition, due to variable distance from the source and slope characteristic (e.g., steepness). The pedological characteristics of this second phase, comparatively to the first phase but in a lesser extent, point to the formation of Luvisols (IUSS Working Group WRB, 2015) under a stable forest cover. Similarly, a second colluvial event interrupted this pedogenetic phase. However, in this case, the deposited material is more homogeneous, as it is mainly composed of claystone fragments (including lithorelicts *sensu* Brewer, 1976) and pedorelicts (*sensu* Brewer, 1976), coming from the B horizons of Luvisols developed during the former pedogenetic phase, then eroded and reworked by geomorphological processes.

- *γ pedogenesis*: the characteristics of the present-day pedogenetic phase suggest a slight change in conditions compared to the previous two phases. The values of the Al_o + ½ Fe_o index calculated for ABt2 and BC horizons of 02 profile seem to evidence a weak podzolization (Do Nascimento et al., 2008; Waroszewski et al., 2013; IUSS Working Group WRB, 2015). However, this process is not recognizable in the

field, and is therefore qualified as cryptopodzolization, forming a "ranker cryptopodzolique" soil (*sensu* Duchaufour, 1983) or a Leptosol (protospodic) (IUSS Working Group WRB, 2015), as already observed in other soils of the Mt. Cusna (Mariani, 2016). This process could be favored by the development of low shrub vegetation dominated by acidophilic species, e.g. *Vaccinium myrtillus* (Duchaufour, 1983; Chersich et al., 2007; Compostella et al., 2013; Mariani, 2016). As far as the other profiles are concerned, under the same vegetation cover, an even less conspicuous process than cryptopodzolization can act, inducing the formation of a "ranker subalpin" soil (Duchaufour, 1983) or an Umbric Leptosol (IUSS Working Group WRB, 2015), except for the 04 profile, located downslope in a forest context, which can be regarded as a "ranker brunifié" soil (Duchaufour, 1983) or a Brunic Leptosol (IUSS Working Group WRB, 2015).

Finally, in some cases, the present-day pedogenesis is superimposed to the previous one (see Section 4.2 of the Discussion), the latter being identifiable by relict and textural pedofeatures (see Section 4.2 of the Discussion), emphasizing a greater inertia (Duchaufour, 1983) than the ongoing pedofeatures development.

4.5. Interactions between the geomorphological context, the Holocene climate variations, and the vegetation changes as influencing factors on paleosols

The study area is characterized during the Holocene by alternating phases of rhexistasy and biostasy (Erhart, 1967). The pedogenesis has been mainly affected by three factors throughout time (i.e., climate, vegetation, slope features), which strongly influenced the environmental evolution of the area. In Fig. 8, a sketch on the role of the main factors influencing the soil development through time in the study area is proposed and herein discussed. The most ancient phase, recorded by the paleosols, was a biostasy phase (α pedogenesis) during which the climate was probably warm with a stable forest vegetation cover at the Mt. Cusna NW slope. Soil processes were mainly governed by a well-developed brunification, together with clay illuviation. Even if the time control of the pedogenetic phases at Mt. Cusna area remains speculative, it is likely that this pedogenetic phase took place in the Early Holocene (see below). Subsequent climate changes and their associated vegetation shift downward the slope caused a phase of strong instability, marked by the action of colluvial processes and the interruption of pedogenetic processes. At a regional scale, in the Italian Apennines, a relationship can be drawn between cold periods and an increase in mass wasting events (Bertolini, 2007). During such a phase, slope processes eroded soils and deposited un-weathered mineral material at the topographic surface. The change to warmer temperatures promoted a new stable phase (β), characterized by similar environmental conditions observed during the previous warm period. According to Cremaschi et al., (1984) and Compostella et al. (2013), this phase could correspond to the Early/Middle Holocene, since in the neighboring area, the charcoals coming from the upper part of soils developed during the β pedogenesis were radiocarbon dated (3920–3700 cal yr BP: Compostella et al., 2013) after the Middle/Late Holocene boundary (Mariani et al., 2019b). The difference in soil development grade, in respect to the previous stable phase, can be attributed to the different duration of pedogenesis or to a different vegetation cover, as testified by the variation in organic material characteristics highlighted by Rock-Eval® parameters. Such change in vegetation was likely driven by human modifications, as in many other parts of Italy and the Mediterranean during this period (Cremaschi and Nicosia, 2010; Regattieri et al., 2019; Sevink et al., 2019). This stability phase was interrupted by slope instability, due to a likely climate deterioration (probably during the LIA: Mariani et al., 2019b; Zerboni et al., 2019) associated to a loss of the vegetation cover, again due to the increased pastoral impact at higher elevations since the Middle Ages (Panizza et al., 1982), coupled with the exploitation of the forest below for charcoal production. However, colluvial processes during this latter phase of rhexistasy seem to have been less intense than the previous one, with soils partially eroded, and in some case, with previously buried paleosols exhumed. Moreover, transported and deposited material was often pre-altered, as it was originating from paleosols developed in higher topographic positions. Finally, the present-day pedogenesis starts from these colluvial deposits and/or from the exhumed paleosols. The present-day phase of biostasy (γ) is characterized by distinctive environmental conditions with a different vegetation cover (i.e., shrubs): present-day soils are apparently less developed, possibly because of the vegetation type (i.e., cryptopodzolization induced by *Vaccinium myrtillus*), colder conditions, or a short duration of pedogenesis (Duchaufour, 1983; Compostella et al., 2014). The sparse vegetation cover, mainly composed of shrubs and apparently not subject to reforestation, does not protect the soil enough from water driven erosion acting today, triggering a soil cover erosion along the edge of rills.

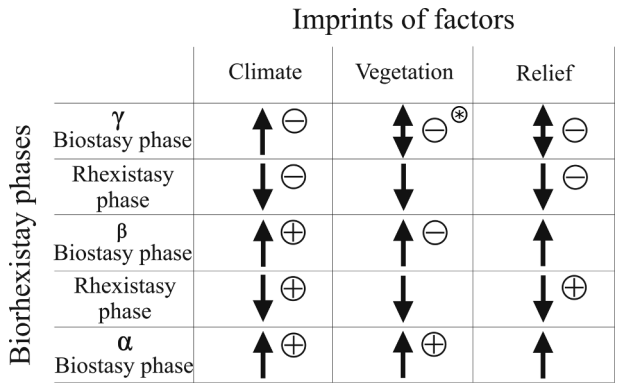

Fig. 8. Role of the main factors influencing the soil development through time in the study area. The upward arrow represents favorable conditions to soil development, whereas the downward arrow represents unfavorable conditions regarding soil development. The presence of plus or minus signs underlines the active role of a factor, which can be more (plus) or less (minus) intense, in its influence on the pedogenesis. *: human impact influence in vegetation cover.

5. Conclusions

This paper presents the assessment of the different environmental conditions that have affected the NW slope of Mt. Cusna, based on the analysis of soils and paleosols. In the Mt. Cusna toposequence, three different soil units have been identified: (i) a first (and the most ancient) soil unit, characterized by a well-developed brunification with clay illuviation, (ii) a second unit, characterized by the same processes of the first unit, but less intense, and (iii) a third recent unit, presenting a weak pedogenesis. This latter, in some case, superimposed on an older truncated soil (paleosol), affecting these exhumed paleosols. Based on the study of these soil units, it has been possible to reconstruct environmental changes that affected the Mt. Cusna slope during the Holocene, to identify the succession of phases of slope stability, during which soils developed, and phases characterized by erosion and deposition processes.

In this light, soils proved to be a useful archive, not only to reconstruct the past environmental conditions, but also to trace the geomorphological processes that affected the area. In addition, it has been possible to identify the role of the geomorphological processes that have affected the evolution of complex paleosol sequences. This work, based on different lab techniques, demonstrated that a multi-analytical approach is necessary to properly characterize soils and their genetic pedological processes; for example, the use of Rock-Eval® pyrolysis improved substantially our knowledge about the relationship between paleosols and organic matter and, as such, opens new research avenues in paleopedogenesis.

Declaration of Competing Interest

The authors declare that they have no known competing financial interests or personal relationships that could have appeared to influence the work reported in this paper.

Acknowledgments

Rock-Eval® is a trademark registered by IFP Energies Nouvelles. This work was supported by Università degli Studi di Milano, Fondi Potenziamento della Ricerca – Linea 2 – 2018 (entrusted to I. M. Bollati). The authors thank the International Relations from the University of Lausanne who provided travel funds between Italy and Switzerland. The authors thank the staff at the University of Lausanne (Switzerland) for completing the Rock-Eval® analyses, and they are particularly grateful to Thierry Adatte (Institute of Earth Sciences) and Stéphanie Grand (Institute of Earth Surface Dynamics) for their technical and scientific supports. The authors are also grateful to Chiara Compostella and Elena Silvia Ferrari for their assistance during the analyses at the Sediments and Soils Laboratory at Earth Science Department of Università degli Studi di Milano. The authors want to thank two anonymous reviewers for their constructive remarks that substantially improved the first version of the manuscript.

Appendix A. Supplementary material

Supplementary data to this article can be found online at https://doi.org/10.1016/j.catena.2020.104951.

References

Albrecht, R., Sebag, D., Verrecchia, E.P., 2015. Organic matter decomposition: bridging the gap between Rock-Eval pyrolysis and chemical characterization (CPMAS 13C NMR). Biogeochemistry 122, 101–111.
Arduino, E., Barberis, E., Ajmone Marsan, F., Zanini, E., Franchini, M., 1986. Iron oxides and clay minerals within profiles as indicators of soil age in northern Italy. Geoderma 37, 45–55.
Avery, B.W., Bascomb, C.L., (Eds.). 1982. Soil survey laboratory methods. Lawes agricultural trust.
Bascomb, C.L., 1968. Distribution of pyrophosphate-extractable iron and organic carbon in soils of various groups. Eur. J. Soil Sci. 19 (2), 251–268.
Behar, F., Beaumont, V., De B. Penteado, H.L., 2001. Rock-Eval® 6 technology: performances and developments. Oil Gas Sci. Technol. 56(2), 111–134.
Biagi, P., Castelletti, L., Cremaschi, M., Sala, B., Tozzi, C., 1980. Popolazione e territorio nell'Appennino ToscoEmiliano e nel tratto centrale del bacino del Po e nelle Prealpi bresciane tra il IX ed il V millennio. Emilia Preromana 8, 13–36.
Bertolini, G., 2007. Radiocarbon dating on landslides in the Northern Apennines (Italy). In: McInnes, R., Jakeways, J., Fairbank, H., Mathie, E. (Eds.), Landslides and Climate Change. Taylor & Francis Group, London.
Bertolini, G., Pellegrini, M., 2001. The landslides of Emilia Apennines (Northern Italy) with reference to those which resumed activity in the 1994–1999 period and required civil protection interventions. Quaderni di Geologia 8 (1), 27–74.
Bollati, I.M., Masseroli, A., Mortara, G., Pelfini, M., Trombino, L., 2019. Alpine gullies system evolution: erosion drivers and control factors. Two examples from the western Italian Alps. Geomorphology 327, 248–263.
Bortolotti, V., 1992. Guide Geologiche Regionali: Appennino Tosco-Emiliano. BE-MA Editrice, Milano.
Brewer, R., 1976. Fabric and Mineral Analysis of Soils. Krieger, Huntington, NY.
Casagrande, A., 1934. Die Aräometer-Methode zur Bestimmung der Kornverteilung von Böden und anderer Materialien. –. Springer, Berlin, pp. 56.
Chersich, S., Galvan, P., Frizzera, L., Scattolin, L., 2007. Variabilità delle forme di humus in due siti campione di pecceta altimontana trentina. Forest@-Journal of Silviculture and Forest. Ecology 4 (2), 220–226.
Coltorti, M., Pieruccini, P., 2006. The last interglacial pedocomplexes in the litho-and morpho-stratigraphical framework of the central-northern Apennines (Central Italy). Quat. Int. 156, 118–132.
Coltorti, M., Pieruccini, P., Arthur, K.J., Arthur, J., Curtis, M., 2019. Geomorphology, soils and palaeosols of the Chencha area (Gamo Gofa, south western Ethiopian Highlands). J. Afr. Earth Sc. 151, 225–240.
Compostella, C., Mariani, G.S., Trombino, L., 2014. Holocene environmental history at the treeline in the Northern Apennines, Italy: A micromorphological approach. Holocene 24 (4), 393–404.
Compostella, C., Trombino, L., Caccianiga, M., 2013. Late Holocene soil evolution and treeline fluctuations in the Northern Apennines. Quat. Int. 289, 46–59.
Cremaschi, M., Nicosia, C., 2010. Corso di Porta Reno, Ferrara (Northern Italy): a study in the formation processes of Urban Deposits. Il Quat. Ital. J. Quat. Sci. 23, 395–408.
Cremaschi, M., Rodolfi, G., 1991. Il suolo - Pedologia nelle scienze della Terra e nella valutazione del territorio. La Nuova Italia Scientifica, Roma.
Cremaschi, M., Trombino, L., Zerboni, A., 2018. Palaeosoils and relict soils: a systematic review. In Interpretation of Micromorphological Features of Soils and Regoliths. Elsevier, pp. 863–894.
Cremaschi, M., Biagi, P., Accorsi, C.A., Bandini Mazzanti, M., Rodolfi, G., Castelletti, L., Leoni, L., 1984. Il sito mesolitico di Monte Bagioletto (Appennino Reggiano) nel quadro delle variazioni ambientali oloceniche dell'Appennino Tosco-Emiliano. Emilia Preromana 9/10, 11-46.
D'Amico, M. E., Catoni, M., Terribile, F., Zanini, E., Bonifacio, E., 2016. Contrasting environmental memories in relict soils on different parent rocks in the south-western Italian Alps. Quat. Int. 418, 61–74.
Dewolf, Y., Bourrié, G., 2008. Les formations superficielles: genèse, typologie, classification, paysages et environnements, ressources et risques. Ellipses.
Do Nascimento, N.R., Fritsch, E., Bueno, G.T., Bardy, M., Grimaldi, C., Melfi, A.J., 2008. Podzolization as a deferralitization process: dynamics and chemistry of ground and surface waters in an Acrisol-Podzol sequence of the upper Amazon Basin. Eur. J. Soil Sci. 59 (5), 911–924.
Douglas, L.A., Thompson, M.L., 1985. Soil Micromorphology and Soil Classification. Soil Science Society of America, Madison, WI.
Duchaufour, P., 1983. Pédologie. 1. Pédogenèse et classification. Masson, Paris.
Erhart, H., 1967. La Genèse des sols en tant que phénomène géologique: esquisse d'une théorie géologique et géochimique, biostasie et rhexistasie: exmaples d'application. Masson.
Fedoroff, N., Courty, M., 2012. Textural features and microfacies expressing temporary and permanent soil water saturation. In: Poch-Claret, R., Casamitjana, M., and Francis, M. (Eds.), Proceedings of the 14th Intern. Working Meet. On Soil Micromporphology, page 1.1.K. Session I. Editions i Publications de la Universitat de Lleida, Spain.
Fedoroff, N., Goldberg, P., 1982. Comparative micromorphology of two late Pleistocene paleosols (in the Paris Basin). Catena 9, 227–251.
Fedoroff, N., Courty, M.A., Thompson, M.L., 1990. Micromorphological evidence of paleoenvironmental change in Pleistocene and Holocene paleosols. In: Developments in Soil Science, vol. 19. Elsevier, pp. 653–665.
Gales, S.J., Hoare, P.G., 1991. Quaternary Sediments: Petrographic Methods for the Study of Unlithified Rocks Belhaven, London, p. 323.
Giraudi, C., 2005. Middle to Late Holocene glacial variations, periglacial processes and alluvial sedimentation on the higher Apennine massifs (Italy). Quat. Res. 64 (2), 176–184.
IUSS Working Group WRB, 2015. World Reference Base for Soil Resources 2014, update 2015 International soil classification system for naming soils and creating legends for soil maps. World Soil Resources Reports No. 106. FAO, Rome.
Jenny, H., 1941. Factors of Soil Formation: A System of Quantitative Pedology. McGraw-Hill Book Company Inc., New York.
Jahn, R., Blume, H.P., Asio, V.B., Spaargaren, O., Schad, P., 2006. Guidelines for soil description. FAO.
Kaiser, K., Schoch, W.H., Miehe, G., 2007. Holocene paleosols and colluvial sediments in Northeast Tibet (Qinghai Province, China): properties, dating and paleoenvironmental implications. Catena 69 (2), 91–102.
Kemp, R.A., 1998. Role of Micromorphology in paleopedological research. Quat. Int. 51–52, 133–141.
Kjeldahl, J., 1883. Neue Methode zur Bestimmung des Stickstoffs in organischen Körpern. J. Anal. Chem. 22, 366–382.
Kleber, A., Terhorst, B., 2013. Mid-latitude Slope Deposits (cover beds), vol. 66 Newnes.
Krasilnikov, P., Calderón, N.E.G., 2006. A WRB-based buried paleosol classification. Quat. Int. 156, 176–188.
Kubiëna, W.L., 1953. Bestimmungsbuch und Systematik der Böden Europas. F. Enke Verlag, Stuttgart.
Lafargue, E., Marquis, F., Pillot, D., 1998. Rock-Eval® 6 applications in hydrocarbon exploration, production, and soil contamination studies. Oil Gas Sci. Technol. 53 (4), 421–437.
Losacco, U., 1949. La glaciazione quaternaria dell'Appennino Settentrionale. Rivista Geografica Italiana 56 (2), 90–152.
Losacco, U., 1982. Gli antichi ghiacciai dell'Appennino settentrionale. Studio morfologico e paleogeografico. Atti della Societa dei Naturalisti e Matematici di Modena 113, 1–24.
Magliulo, P., Terribile, F., Colombo, C., Russo, F., 2006. A pedostratigraphic marker in the geomorphological evolution of the Campanian Apennines (Southern Italy): The Paleosol of Eboli. Quat. Int. 156, 97–117.
Malou, O.P., Sebag, D., Moulin, P., Chevallier, T., Badiane-Ndour, N.Y., Thiam, A., Chapuis-Lardy, L., 2020. The Rock-Eval signature of soil organic carbon in arenosols of the Senegalese groundnut basin. How do agricultural practices matter? Agric. Ecosyst. Environ. 301 (107030).
Mariani, G.S., Brandolini, F., Pelfini, M., Zerboni, A., 2019a. Mapping Matilda's castles in the northern Apennines: geological and geomorphological constrains. J. Maps 15 (2), 521–529.
Mariani, G.S., Compostella, C., Trombino, L., 2019b. Complex climate-induced changes in soil development as markers for the Little Ice Age in the Northern Apennines (Italy). Catena 181, 104074.
Mariani, G.S., Cremaschi, M., Zerboni, A., Zuccoli, L., Trombino, L., 2018. Geomorphology of the Mt. Cusna Ridge (Northern Apennines, Italy): evolution of a Holocene landscape. J. Maps 14 (2), 392–401.
Mariani, G.S., 2016. The role of paleosols in paleoenvironmental studies: genesis and development of Apennine mountain soils during the Holocene. Phd Thesis. University of Milan.
Matteodo, M., Grand, S., Sebag, D., Rowley, M.C., Vittoz, P., Verrecchia, E.P., 2018.

Decoupling of topsoil and subsoil controls on organic matter dynamics in the Swiss Alps. Geoderma 330, 41–51.
McCarthy, P.J., Martini, I.P., Leckie, D.A., 1998. Use of micromorphology for palaeoenvironmental interpretation of complex alluvial palaeosols: an example from the Mill Creek Formation (Albian), southwestern Alberta, Canada. Palaeogeogr. Palaeoclimatol. Palaeoecol. 143, 87–110.
Milne, G., 1936. Normal erosion as a factor in soil profile development. Nature 138 (3491), 548.
Ministero delle Risorse Agricole Alimentari e Forestali, 1994. Metodi ufficiali di 1036 analisi chimica del suolo, con commenti ed interpretazioni. ISMEA, Roma, 207 pp.
Nicosia, C., 2006. Indicatori micromorfologici di erosione dei suoli nel settore settentrionale delle Valli Grandi Veronesi durante l'età del Ferro. Padusa 62, 108–112.
Panizza, M., Bettelli, G., Bollettinari, G., Carton, A., Castaldini, D., Piacente, S., Bernini, M., Clerici, A., Tellini, C., Vittorini, S., Canuti, P., Moisello, U., Tenti, G., Dramis, F., Gentili, B., Pambianchi, G., Bidini, D., Lulli, L., Rodolfi, G., Busoni, E., Ferrari, G., Cremaschi, M., Marchesini, A., Accorsi, C.A., Mazzanti, M., Francavilla, F., Marchetti, G., Vercesi, P.L., Di Gregorio, F., Marini, A., (Gruppo Ricerca Geomorfologia CNR) 1982. Geomorfologia del territorio di Febbio tra il M.Cusna e il F.Secchia (Appennino Emiliano). Geografia Fisica Dinamica Quaternaria 5, 285–360.
Pawluk, S., 1972. Measurement of crystalline and amorphous iron removal in soils. Can. J. Soil Sci. 52, l19–l123.
Regattieri, E., Zanchetta, G., Isola, I., Zanella, E., Drysdale, R.N., Hellstrom, J.C., Zerboni, A., Dallai, L., Tema, E., Lanci, L., et al., 2019. Holocene Critical Zone dynamics in an Alpine catchment inferred from a speleothem multiproxy record: disentangling climate and human influences. Sci. Rep. 9, 1–9.
Rellini, I., Trombino, L., Firpo, M., Piccazzo, M., 2007. Geomorphological context of "plinthitic paleosols" in the Mediterranean region: examples from the coast of western Liguria (northern Italy). Rev. C. & G. 21 (1–2), 27–40.
Rhodes, E.R., Sutton, P.M., 1978. Active iron ratio of some soils from three physiographic units in Sierra Leone. Soil Sci. 125 (5), 326–328.
Romanens, R., Pellacani, F., Mainga, A., Fynn, R., Vittoz, P., Verrecchia, E.P., 2019. Soil diversity and major soil processes in the Kalahari basin, Botswana. Geoderma Reg. 19, e00236. https://doi.org/10.1016/j.geodrs.2019.e00236.
Ruellan, A., 1971. The history of soils. Some problems of definition and interpretation. In: Yaalon, D.H. (Ed.), Paleopedology. Origin, Nature and Dating of Paleosols. Israel University Press, Jerusalem, 350 pp.
Sauro, U., Ferrarese, F., Francese, R., Miola, A., Mozzi, P., Rondo, G.Q., Trombino, L., Valentini, G., 2009. Doline fills- case study of the Faverghera Plateau (Venetian Pre-Alps, Italy). Acta Carsologica 38(1), 51–63.
Schomburg, A., Verrecchia, E.P., Guenat, C., Brunner, P., Sebag, D., Le Bayon, R.C., 2018. Rock-Eval® pyrolysis discriminates soil macro-aggregates formed by plants and earthworms. Soil Biol. Biochem. 117, 117–124.
Schomburg, A., Sebag, D., Turberg, P., Verrecchia, E. P., Guenat, C., Brunner, P., Adatte T, Schlaepfer R., Le Bayon, R. C., 2019. Composition and superposition of alluvial deposits drive macro-biological soil engineering and organic matter dynamics in floodplains. Geoderma 355, 113899.
Schwertmann, U., 1973. Use of oxalate for Fe extraction from soils. Can. J. Soil Sci. 53 (2), 244–246.
Sebag, D., Verrecchia, E.P., Cécillon, L., Adatte, T., Albrecht, R., Aubert, M., Bureau, F., Cailleau, G., Copard, Y., Decaens, T., Disnar, J.R., Hetényi, M., Nyilas, T., Trombino, L., 2016. Dynamics of soil organic matter based on new Rock-Eval® indices. Geoderma 284, 185–203.
Sevink, J., Bakels, C.C., Attema, P.A., Di Vito, M.A., Arienzo, I., 2019. Holocene vegetation record of upland northern Calabria, Italy: Environmental change and human impact. The Holocene 29, 633–647.
Sheldon, N.D., Tabor, N.J., 2009. Quantitative paleoenvironmental and paleoclimatic reconstruction using paleosols. Earth Sci. Rev. 95 (1–2), 1–52.
Stoops, G., 2003. Guidelines for analysis and description of soil and regolith thin sections. Soil Science Society of America, Inc., Madison, Wisconsin, USA.
Stoops, G., Marcelino, V., Mees, F., 2018. Interpretation of Micromorphological Features of Soils and Regoliths. Elsevier.
Stoops, G., Marcelino, V., Mees, F., 2010. Interpretation of Micromorphological Features of Soils and Regoliths. Elsevier.
Thoumazeau, A., Chevallier, T., Baron, V., Rakotondrazafy, N., Panklang, P., Marichal, R., Kibblewhite, M., Sebag, D., Tivet, F., Bessou, C., Gay, F., Brauman, A., 2020. A new in-field indicator to assess the impact of land management on soil carbon dynamics. Geoderma 375, 114496.
Vittori Antisari, L., Bianchini, G., Cremonini, S., Di Giuseppe, D., Falsone, G., Marchesini, M., Marvelli, S., Vianello, G., 2016. Multidisciplinary study of a late glacial-Holocene sedimentary sequence near Bologna (Italy): insights on natural and anthropogenic impacts on the landscape dynamics. J. Soils Sediments 16, 645–662.
Walkley, A., Black, I.A., 1934. An examination of the Degtjareff method for determining soil organic matter, and proposed modification of the chromic acid titration method. Soil Sci. 37 (1), 29–38.
Waroszewski, J., Kalinski, K., Malkiewicz, M., Mazurek, R., Kozlowski, G., Kabala, C., 2013. Pleistocene-Holocene cover-beds on granite regolith as parent material for Podzols—an example from the Sudeten Mountains. Catena 104, 161–173.
Zanelli, R., Egli, M., Mirabella, A., Giaccai, D., Abdelmoula, M., 2007. Vegetation effects on pedogenetic forms of Fe, Al and Si and on clay minerals in soils in southern Switzerland and northern Italy. Geoderma 141 (1–2), 119–129.
Zanini, E., Freppaz, M, Stanchi, S, Bonifacio, E, Egli, M., 2015. Soil variability in mountain areas. In: Romeo, R; Vita, A; Manuelli, S; Zanini, E; Freppaz, Michele; Stanchi, Silvia. Understanding Mountain Soils: A Contribution from mountain areas to the International Year of Soils 2015. FAO, Rome, pp. 60–62.
Zerboni, A., Mariani, G.S., Castelletti, L., Amit, R., Ferrari, E.S., Tremari, M., Livio, F., 2019. Was the Little Ice Age the coolest Holocene climatic period in the Italian central Alps? Prog. Phys. Geogr. https://doi.org/10.1177/0309133319881105.